# Supporting Information

## In-situ Preparation $Bi_2O_2Se/MoO_3$ Thin-Film Heterojunction Flexibility Array Photodetectors

Ming Yang[a,b,e]*, Xiaoqiang Zhang[a], Hongxi Zhou[b,c], Gui Fu[a], Xin Zhou[b,c], Yunlun Lian[b], Jinxin Hao[d], He Yu[b,c], Xinyu Zhu[a] and Jun Wang[a,b,c,]*

[a] *Institute of Electronic and Electrical Engineering, Civil Aviation Flight University of China,*
*Guanghan, 618307, P.R. China*

[b] *School of Optoelectronic Science and Engineering, University of Electronic Science and Technology of China*
*Chengdu 610054, P.R. China*

[c] *State Key Laboratory of Electronic Thin films and Integrated Devices, University of Electronic Science and Technology of China,*
*Chengdu 610054, P.R. China*

[d] *Engineering Techniques Training Center, Civil Aviation University of China,*
*Tianjin 300300, P.R. China*

[e] *Sichuan Province Engineering Technology Research Center of General Aircraft Maintenance, Civil Aviation Flight University of China,*
*Guanghan 618307, P.R. China*

*Corresponding Authors:*

*E-mail:yangming932@163.com (M. Yang); wjun@uestc.edu.cn (J. Wang)*

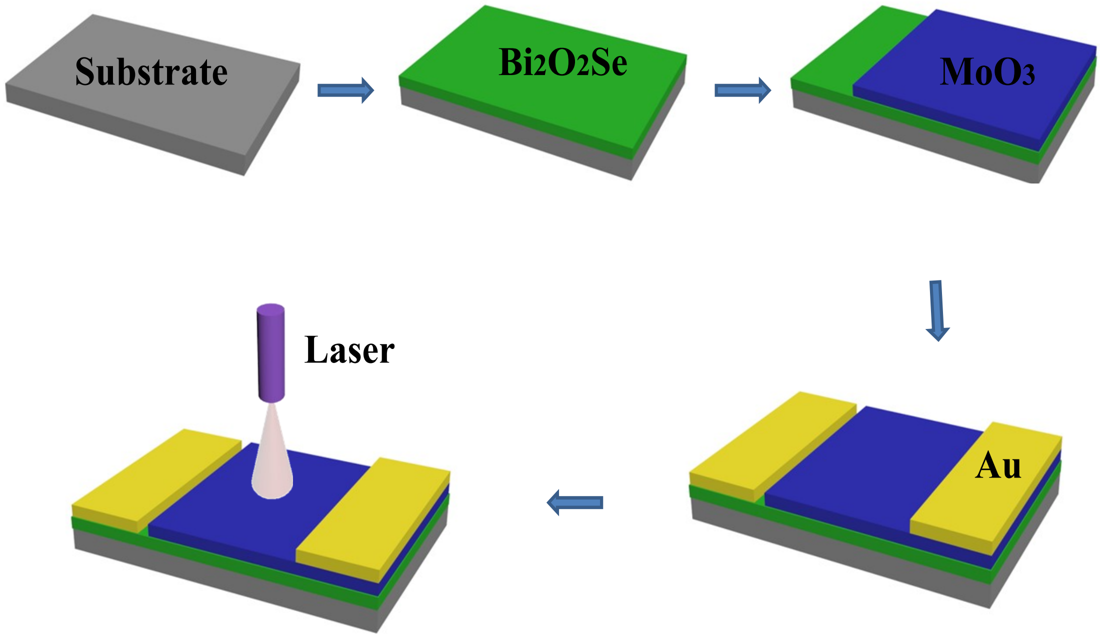


**Figure S1.** Schematic diagram of the fabrication process of $Bi_2O_2Se/MoO_3$ composite thin film and device by two-step thermal deposition method.

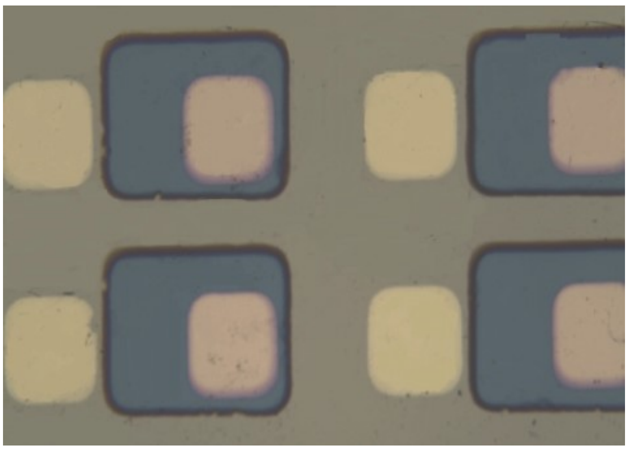

**Figure S2.** Optical image of $Bi_2O_2Se/MoO_3$ thin film array heterojunction device on mica.

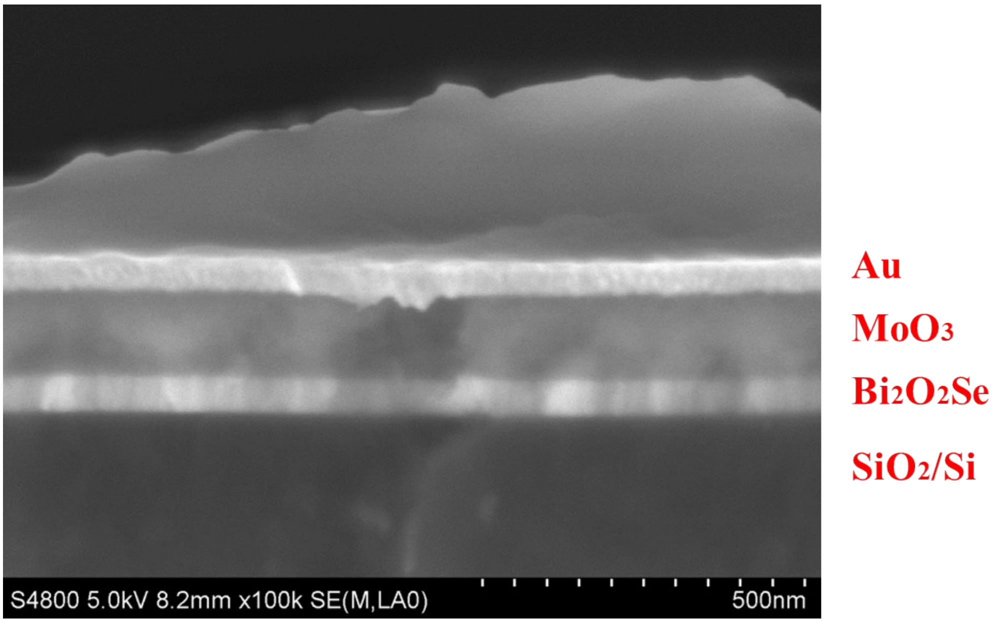


**Figure S3.** Cross section SEM image of the fabricated $Bi_2O_2Se/MoO_3$ thin film heterojunction device.

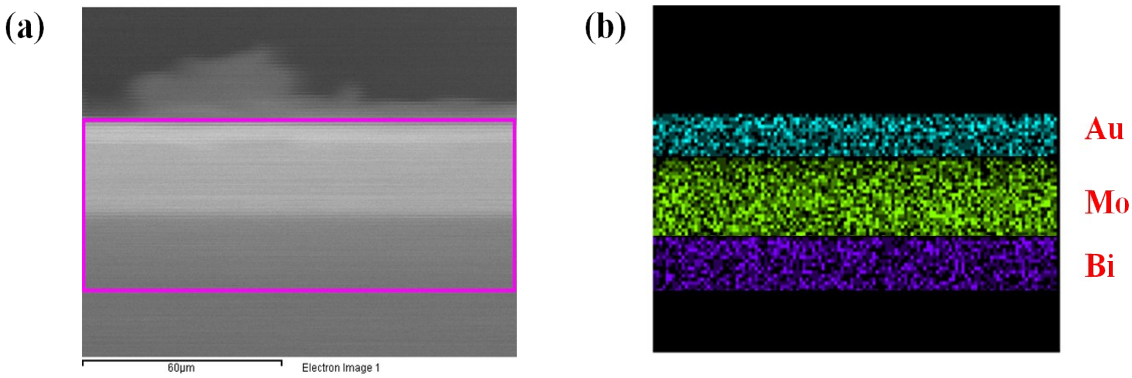


**Figure S4.** The EDS cross section element mapping image of the fabricated $Bi_2O_2Se/MoO_3$ thin film heterojunction device.

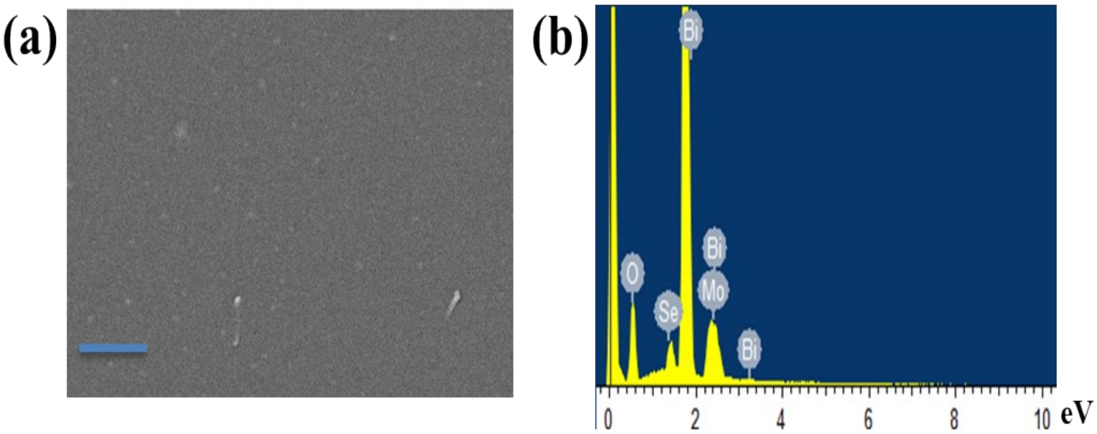


**Figure S5.** The SEM image (a) and EDS pattern (b) of $Bi_2O_2Se/MoO_3$ heterostructure.

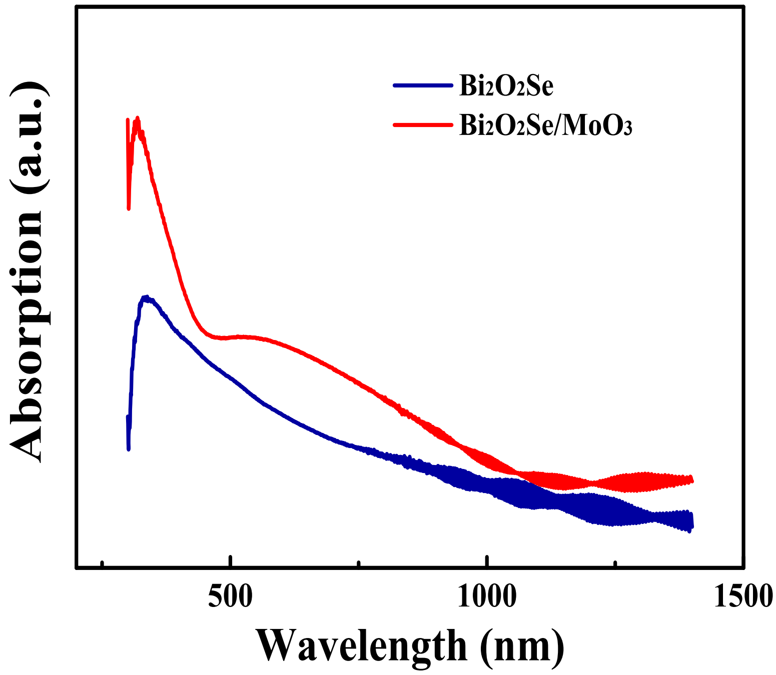


**Figure S6.** Absorption curves of $Bi_2O_2Se/MoO_3$ and $Bi_2O_2Se$ thin films from 300 nm to 1400 nm.

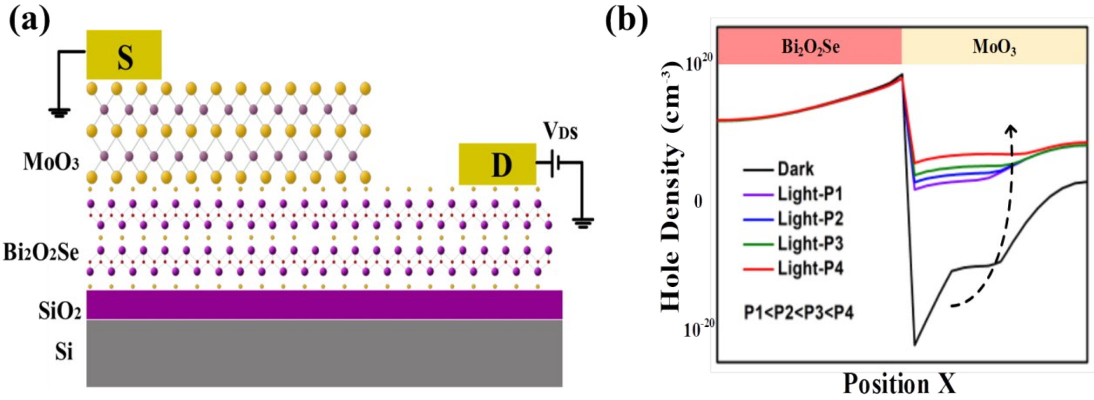


**Figure S7.** (a) The $Bi_2O_2Se/MoO_3$ thin films heterojunction device structure simulate diagram of SILVACO TCAD software. (b) The holes density diagram of $Bi_2O_2Se/MoO_3$ thin films heterojunction device by SILVACO TCAD software simulate @ 808 nm irradiation with different power intensity.

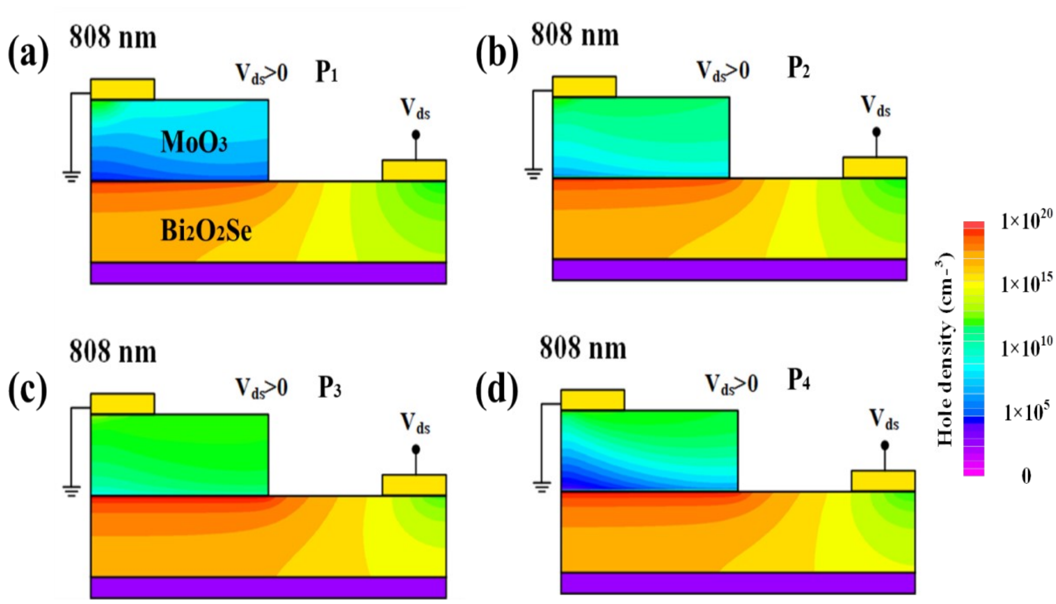


**Figure S8.** The holes distribution density diagram of $Bi_2O_2Se/MoO_3$ thin films heterojunction device by SILVACO TCAD software simulate under 808 nm irradiation with different power intensity (a) P1, (b) P3, (c) P2 and (d) P4. Among $P_4 > P_3 > P_2 > P_1$.

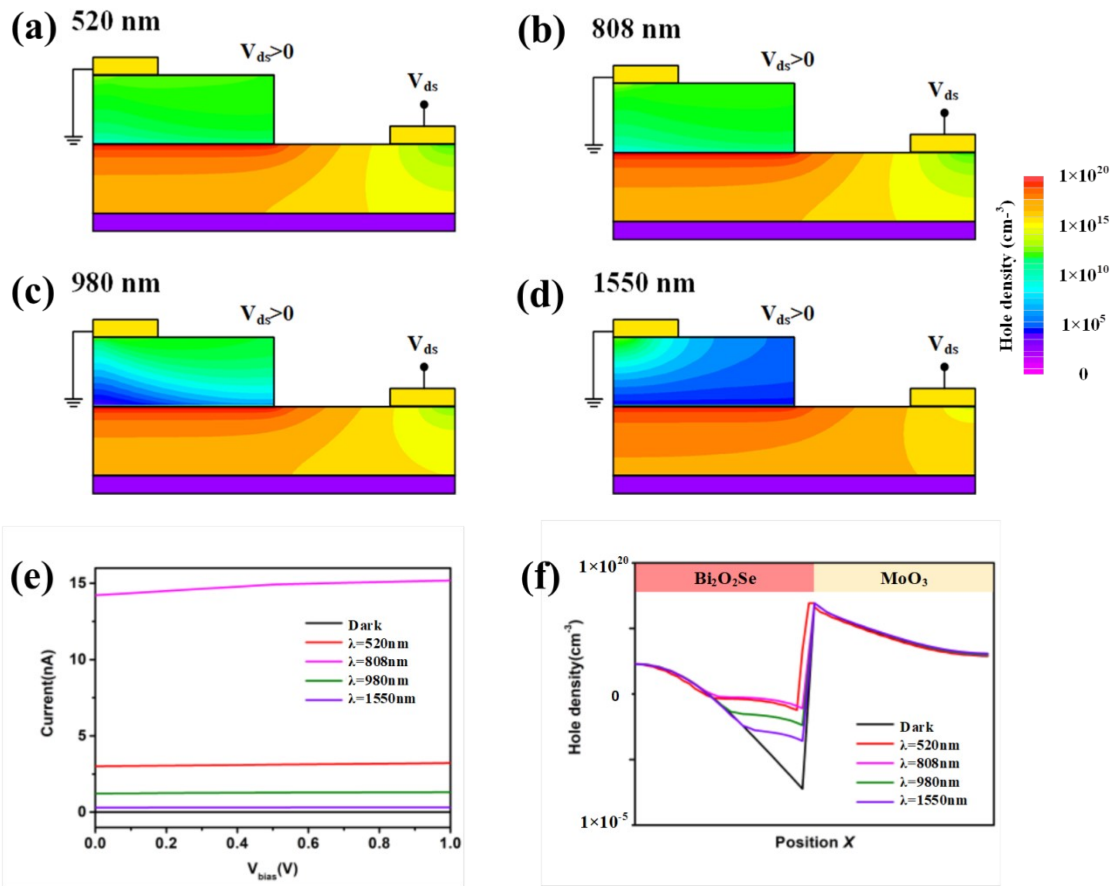


**Figure S8.** The holes distribution density diagram of $Bi_2O_2Se/MoO_3$ thin films heterojunction device by SILVACO TCAD software simulate under $V_{ds} > 0$ V with different waveband light irradiation (a) 520 nm, (b) 808 nm, (c) 980 nm and (d) 1550 nm. (e), (f) Current and holes distribution density curves of $Bi_2O_2Se/MoO_3$ thin films heterojunction device.

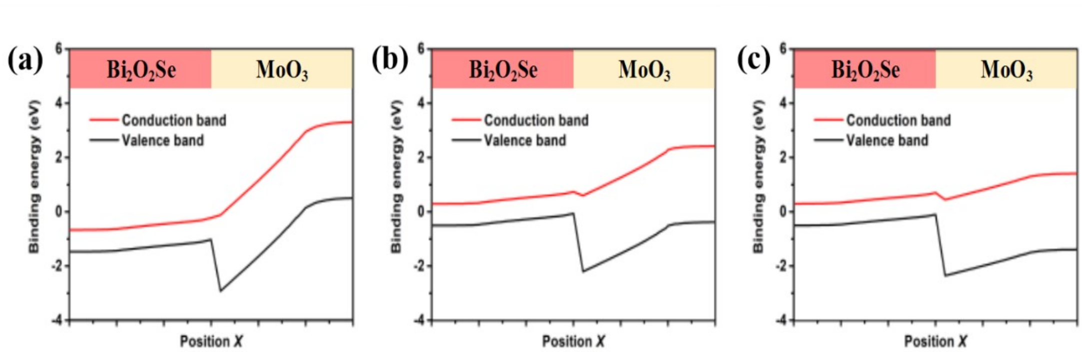


**Figure S10.** The band contact diagram of $Bi_2O_2Se$ and $MoO_3$ materials under (a) $V_{ds} < 0$ V, (b) $V_{ds} = 0$ V and (c) $V_{ds} > 0$ V according to the band characteristics.

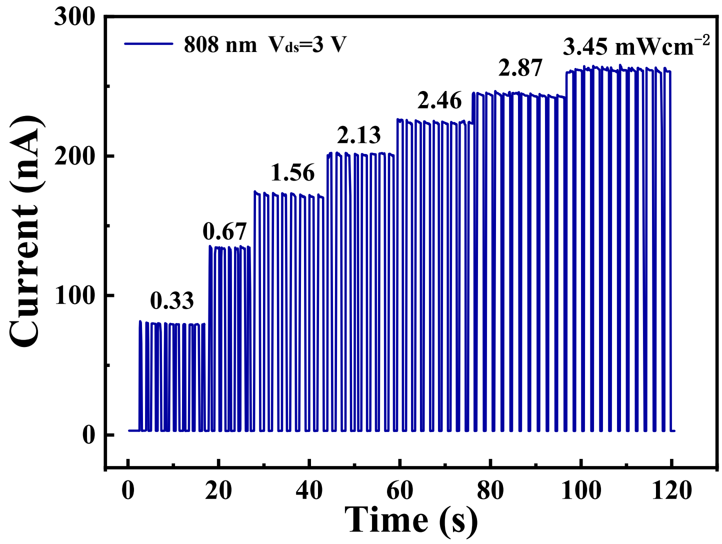


**Figure S11.** $I_{ph}$ of $Bi_2O_2Se/MoO_3$ device @ 808 nm under different power densities.

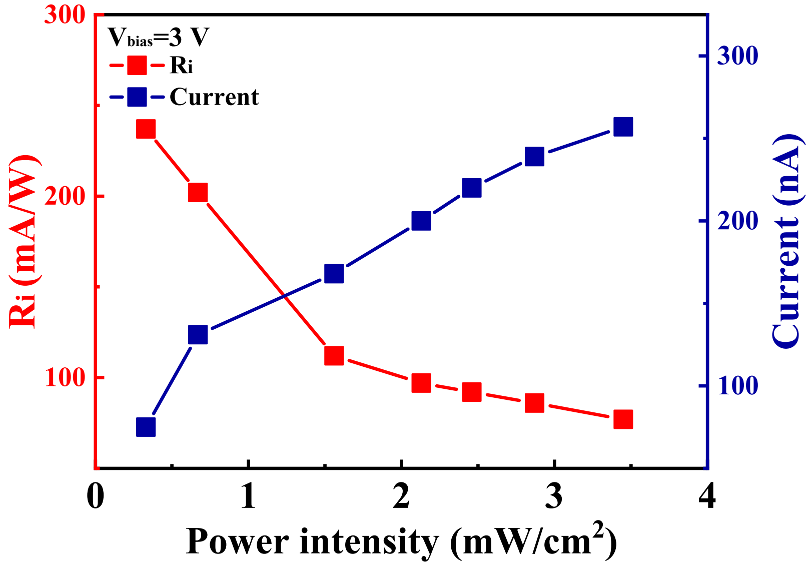


**Figure S12.** $R_i$ and current curves of $Bi_2O_2Se/MoO_3$ device at different laser power intensity.

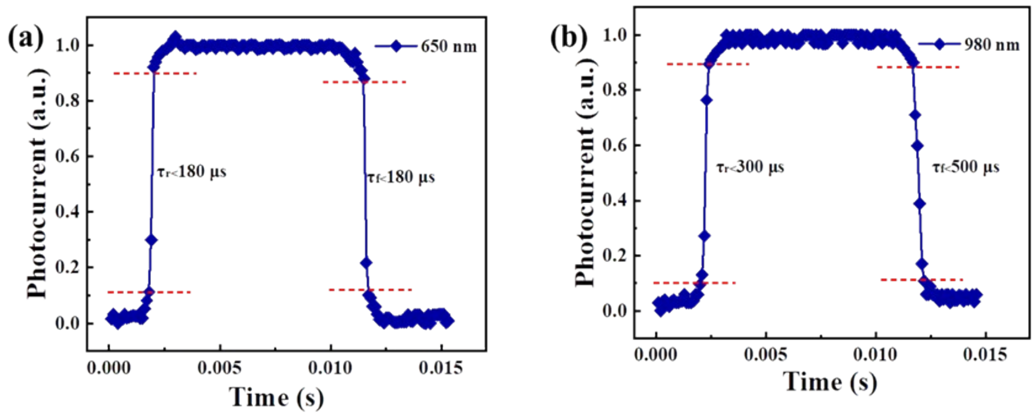


**Figure S13.** $\tau_{on}$ and $\tau_{off}$ of the $Bi_2O_2Se/MoO_3$ heterojunction photodetector (a) @ 650 nm and (b) @ 980 nm. The $\tau_{on}$ and $\tau_{off}$ of device @ 650 nm and @ 980 nm were less than 180 and 180 μs, 300 and 500 μs, respectively.

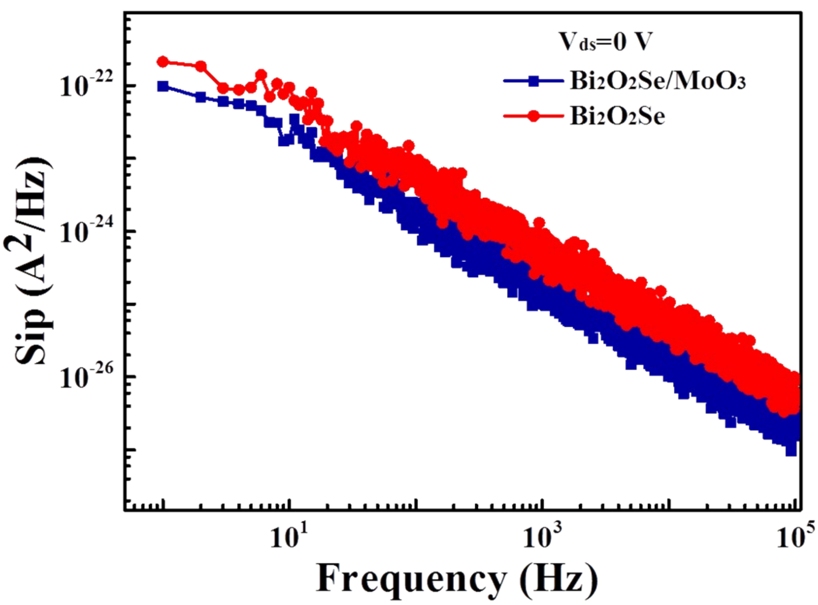


**Figure S14.** The noise diagram of pure $Bi_2O_2Se$ thin film device and $Bi_2O_2Se/MoO_3$ thin film heterojunction device.

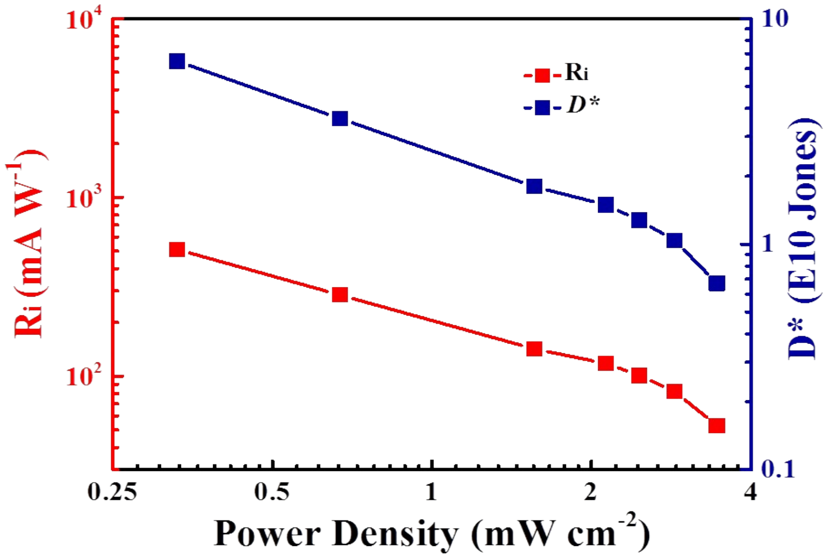


**Figure S15.** The relationship between the $R_i$ and *D** of the $Bi_2O_2Se/MoO_3$ thin film heterojunction device and the laser power density changes.